International Journal of Fracture **40**: 1–12, 1989.

Shear band characterization of mixed mode I and II fully plastic crack growth

G.A. KARDOMATEAS* and F.A. McCLINTOCK
Massachusetts Institute of Technology, Cambridge, Massachusetts 02139, USA
(**present address: General Motors Research Laboratories, Engineering Mechanics Department, Warren, Michigan 48090-9055, USA*)

Received 30 January 1988; accepted 27 July 1988

Abstract. Fully plastic crack growth in singly-grooved plane strain tensile specimens is here characterized by the directions and amounts of fracture and slip on three planes. This model gives the crack growth ductility, defined as the axial displacement per unit ligament reduction (of practical importance in determining the stiffness of the surrounding structure that is needed to prevent unstable fracture) in terms of the fracture surface lengths and directions, as well as the deformation of the back surface. It also gives the directions and magnitudes of slip and fracture.

Applied to six different structural alloys with strain-hardening exponents from 0.1 to 0.2, the model gave crack growth ductilities within 10 percent of the observed ones for the symmetrical configurations, where the values ranged from 0.25 to 0.40 and were unrelated to the strain-hardening exponent. For the asymmetrical configurations (that could occur near welds or shoulders), the crack growth ductility for the low hardening materials drops from 0.07 to 0.11. The predicted values (larger for the higher hardening alloys) were within 30 percent of the observed ones. Thus this slip plane model of fully plastic crack growth provides a useful correlation between macroscopic measurements made on the specimens after fracture, and the important loss of crack growth ductility that occurs in fully plastic asymmetric configurations with low strain-hardening materials.

1. Introduction

If a structure cracks, it is desirable that any crack growth be fully plastic to provide large deflections, both for stability by load-shedding to other parts of the structure, and for facilitating crack detection before failure of the entire structure. This desired crack growth ductility is reduced by asymmetry, which tends to focus the deformation into a single band, along which the crack advances into pre-damaged material. With symmetry, on the other hand, the crack tends to advance between two slip bands into undamaged material (Fig. 1). Kardomateas and McClintock [1] have found that for plane strain tension applied to singly-grooved specimens of low strain-hardening alloys (strain-hardening exponent $n \simeq 0.1$), asymmetric (mixed mode I and II) specimens showed only 1/3 the crack growth ductility of symmetric (mode I) ones. This reduction is much less pronounced for crack initiation and for high hardening alloys ($n \simeq 0.2$). The object here is to characterize the local sliding-off and fracture processes in terms of macroscopic observations of deformation.

Strain-hardening materials require a finite element analysis, perhaps coupled with a rigid-plastic singularity [2], and in turn at the very tip, if not dominated by the fracture process zone itself, an elastic–plastic singularity (Ponte-Castañeda [3]). Even when these analyses can be successfully combined, there will be a need for an approximate characterization in simple terms. Here we consider such an analysis based on at most two shear bands from the tip of a growing crack. In symmetrical, singly-grooved specimens of non-hardening

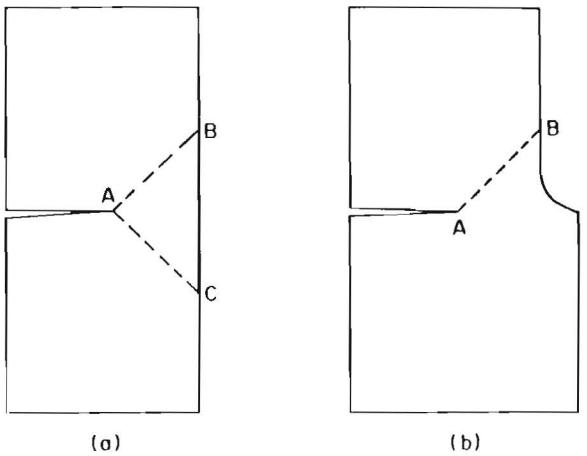

Fig. 1. Symmetric (a) and asymmetric (b) shear band configurations from cracks.

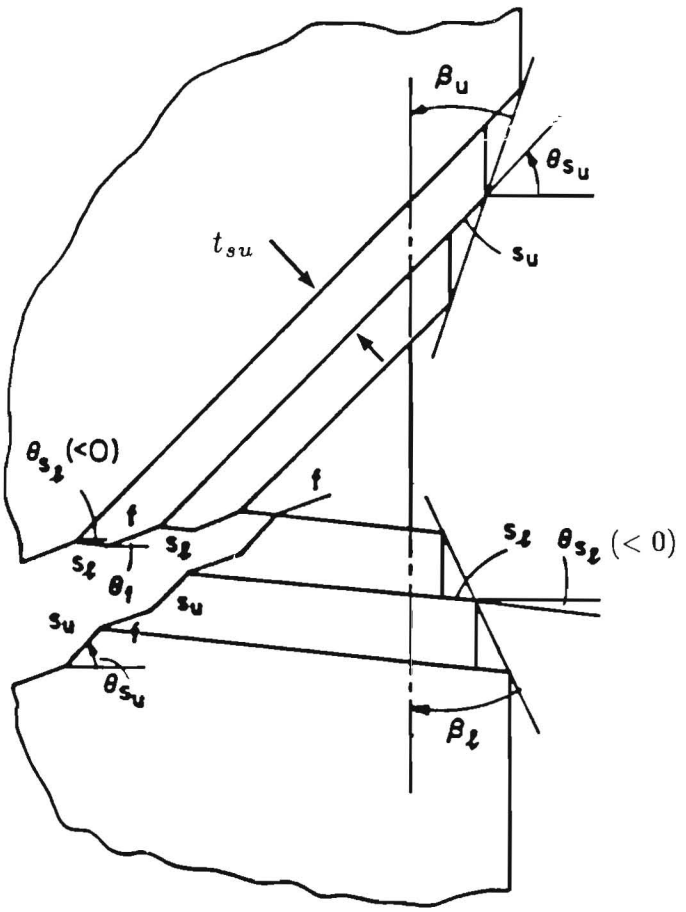

Fig. 2. Details of crack growth by alternating slip on two planes, one below and one above the transverse, and fracture on a plane between the two slip planes.

material, there are two bands at ± 45 deg. In doubly-grooved specimens under tension, or for strain hardening materials, the deformation may occur in a fan, which would be approximated by a slip band at other than 45 deg from the axis.

Crack growth is a mixture of sliding off and cracking [4]. Here it is idealized by assuming cycles of first sliding off an upper slip plane, then on a lower, and finally fracture on possibly a third (Fig. 2). The combination of cracking and sliding off gives the two new surfaces of the macro fracture. These define the crack opening angle and the crack direction. These ideas will now be developed quantitatively, giving a description of the mixed mode ductile crack growth based on an idealization of the underlying physical mechanisms. The model will be an extension of the single band pure mode II asymmetric case [5] and it will also include the crack growth ductility, which is the axial displacement per unit load drop (at the same time Eqn. (9) of that analysis, for the back angle, is corrected here). This crack growth ductility is of interest in determining the stiffness of the surrounding structure that is needed for stable crack growth. It should be emphasized that our objective is a characterization, based on a two-slip model that is characteristic of low-hardening, low triaxiality, situations. Sufficient strain-hardening will distort the relation of micro-mechanical to far-field values, and triaxiality will reduce the strains to fracture and hence the crack growth ductility.

2. Analysis

Consider lower and upper slip planes at angles θ_{sl} and θ_{su} (Fig. 2). The lower flank is formed by sliding off along the upper slip plane at θ_{su} and the fracture f at θ_f. For the moment assume $\theta_{sl} < 0 < \theta_f < \theta_{su}$. Then the upper crack flank is formed by sliding off along the lower slip plane at θ_{sl}, through a distance s_l combined with fracture over a distance f at an angle θ_f. As independent micro-mechanical variables, consider the cracking and shearing parameters f, s_u, s_l, the fracture angle θ_f, and the slip angles θ_{sl}, θ_{su}. The limiting mode I case, with two symmetric slip lines, corresponds to $\theta_f = 0$, $\theta_{su} = -\theta_{sl} = 45°$, and $s_l = s_u$. The limiting mode II case of slip on a single plane corresponds to $s_l = 0$ and $\theta_{su} = 45$ deg.

Six observable quantities that allow solving for the physical variables turn out to be the angles between the faces of the crack and the transverse direction, θ_u, θ_l, the transverse components of the crack flanks after complete separation, l_u, l_l, the initial liagament, l_0, and the angle β_u that the deformed upper back surface makes to the load axis (Fig. 3). Other dependent variables of interest are the total axial displacement per initial ligament u_y/l_0, the orientation of the displacement vector ϕ, and the angle that the deformed lower back surface makes to the load axis β_l (Fig. 3). These can be deduced from the analysis and observed from the tests (except the lower back angle, which is suppressed by the shoulder, even though lower slip s_l may occur near the crack tip in hardening materials). Notice that the crack opening angle is $\omega = \theta_l - \theta_u$.

From the six observable quantities, the orientations of the crack flanks θ_u and θ_l from the transverse direction can be found from

$$\tan \theta_u = \frac{f \sin \theta_f + s_l \sin \theta_{sl}}{f \cos \theta_f + s_l \cos \theta_{sl}}, \tag{1a}$$

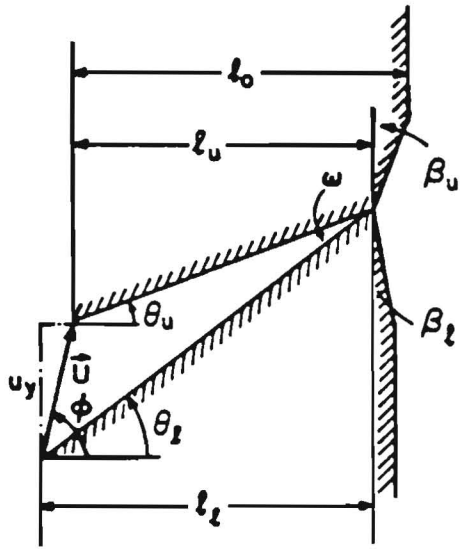

Fig. 3. Macroscopic geometry.

$$\tan \theta_l = \frac{f \sin \theta_f + s_u \sin \theta_{su}}{f \cos \theta_f + s_u \cos \theta_{su}}. \tag{1b}$$

The original ligament thickness l_0, projected onto the transverse direction, is reduced to zero by the cracking f and the sliding s_l and s_u (Fig. 2), and thus provides another relation between the micro-mechanical variables:

$$l_0 = f \cos \theta_f + s_u \cos \theta_{su} + s_l \cos \theta_{sl}. \tag{2}$$

The transverse flank lengths after fracture (projections on the transverse direction) can be measured. The upper and lower flank lengths l_u, l_l, are

$$l_u = f \cos \theta_f + s_l \cos \theta_{sl}, \tag{3a}$$

$$l_l = f \cos \theta_f + s_u \cos \theta_{su}. \tag{3b}$$

The final independent macroscopically observable quantity is taken to be the back angle β, defined as the angle that the deformed back surface makes to the load axis. For the upper surface, from Fig. 2

$$\tan \beta_u = \frac{s_u \cos \theta_{su}}{[f \sin (\theta_{su} - \theta_f) + s_l \sin (\theta_{su} - \theta_{sl})]/\cos \theta_{su} + s_u \sin \theta_{su}}. \tag{4}$$

The dependent (observable) quantity of most interest is the crack growth ductility, defined as the axial displacement per unit ligament reduction. The axial extension is

$$u_y = s_u \sin \theta_{su} - s_l \sin \theta_{sl}. \tag{5}$$

Dividing (5) by (2) gives the crack growth ductility:

$$D_g = \frac{u_y}{l_0} = \frac{s_u \sin \theta_{su} - s_l \sin \theta_{sl}}{f \cos \theta_f + s_u \cos \theta_{su} + s_l \cos \theta_{sl}}. \tag{6}$$

Of interest also is the orientation of the displacement vector from the transverse, ϕ. In terms of the flank lengths and angles, it can be found from

$$\tan \phi = \frac{(l_l/l_0) \tan \theta_l - (l_u/l_0) \tan \theta_u}{l_l/l_0 - l_u/l_0}. \tag{7}$$

Another dependent variable, of interest in fractographic observations, is the apparent crack ductility of the flanks, defined as the projection of the shear-exposed surface onto the total flank surface. It has been roughly estimated fractographically as the ratio of hole growth to sliding-off area [6]. Expressions for the lower and upper apparent crack ductilities are

$$D_{AC,l} = \frac{s_u \cos (\theta_{su} - \theta_l)}{s_u \cos (\theta_{su} - \theta_l) + f \cos (\theta_f - \theta_l)}, \tag{8a}$$

$$D_{AC,u} = \frac{s_l \cos (\theta_{sl} - \theta_u)}{s_l \cos (\theta_{sl} - \theta_u) + f \cos (\theta_f - \theta_u)}. \tag{8b}$$

Less directly observable variables include the lower back angle, which may be suppressed by a shoulder that induces the asymmetry. From Fig. 2, as for the upper back angle,

$$\tan \beta_l = \frac{s_l \cos \theta_{sl}}{[f \sin (\theta_{sl} - \theta_f) + s_u \sin (\theta_{sl} - \theta_{su})]/\cos \theta_{sl} + s_l \sin \theta_{sl}}. \tag{9}$$

Some measure of how sorely tried the non-hardening assumption is can be found from the thickness of the slip bands and the strain in them, found from Fig. 2. For the upper shear band,

$$t_{su} = f \sin (\theta_{su} - \theta_f) + s_l \sin (\theta_{su} - \theta_{sl}), \tag{10a}$$

$$\gamma_u = \frac{s_u}{t_{su}} = \frac{s_u}{f \sin (\theta_{su} - \theta_f) + s_l \sin (\theta_{su} - \theta_{sl})}. \tag{10b}$$

Similarly, for the lower shear band,

$$t_{sl} = f \sin (\theta_f - \theta_{sl}) + s_u \sin (\theta_{su} - \theta_{sl}), \tag{11a}$$

$$\gamma_l = \frac{s_l}{t_{sl}} = \frac{s_l}{f \sin (\theta_f - \theta_{sl}) + s_u \sin (\theta_{su} - \theta_{sl})}. \tag{11b}$$

There are six independent macroscopically observable parameters: the flank angles θ_u, θ_l, the projected flank lengths l_u, l_l, the initial ligament l_0, and the back angle β_u. Equations (1) through (4) determine the corresponding physical variables f, s_l, s_u, θ_f, θ_{sl}, θ_{su}. A suitable algebraic manipulation of the equations can give the solution directly. First define fracture and slip parameters that are projected on planes normal to the tensile axis and normalized with respect to the initial ligament thickness:

$$\tilde{f}_p = f\cos\theta_f/l_0; \quad \tilde{s}_{up} = s_u\cos\theta_{su}/l_0; \quad \tilde{s}_{lp} = s_l\cos\theta_{sl}/l_0. \tag{12}$$

From (2) and (3),

$$\tilde{s}_{up} = 1 - l_u/l_0; \quad \tilde{s}_{lp} = 1 - l_l/l_0; \quad \tilde{f}_p = l_u/l_0 + l_l/l_0 - 1. \tag{13}$$

Thus the upper and lower slip ratios turn out to be directly the upper and lower thinning ratios. There remain three linear equations in $\tan\theta_f$, $\tan\theta_{su}$, and $\tan\theta_{sl}$, which from (1) and (4), with $\tilde{s}_{up} + \tilde{s}_{lp} + \tilde{f}_p = 1$ from (13), are

$$\tilde{f}_p\tan\theta_f + \tilde{s}_{lp}\tan\theta_{sl} = (\tilde{f}_p + \tilde{s}_{lp})\tan\theta_u, \tag{14a}$$

$$\tilde{f}_p\tan\theta_f + \tilde{s}_{up}\tan\theta_{su} = (\tilde{f}_p + \tilde{s}_{up})\tan\theta_l, \tag{14b}$$

$$-\tilde{f}_p\tan\theta_f - \tilde{s}_{lp}\tan\theta_{sl} + \tan\theta_{su} = \tilde{s}_{up}/\tan\beta_u. \tag{14c}$$

For the analysis to be valid, the lower slip angle θ_{sl} should be below the transverse axis (<0). Eliminating θ_{su} and θ_f from (14c) with (14a, b) gives

$$\tan\theta_{sl} = \frac{1}{1 - l_l/l_0}\left[\frac{l_u}{l_0}\left(2 - \frac{l_u}{l_0}\right)\tan\theta_u - \frac{l_l}{l_0}\tan\theta_l + \left(1 - \frac{l_u}{l_0}\right)^2\frac{1}{\tan\beta_u}\right] < 0. \tag{15}$$

This requirement becomes more critical and likely to fail for small crack opening angles, typical of the low hardening asymmetric case. Thus in this case a careful and accurate data reduction, especially in measuring the projected flank lengths, is needed. Unavoidable uncertainties are determining the exact point where the growth zone starts (after the fatigue pre-crack) or ends (i.e. breaks through at the back surface). As a further suggestion, a fitting procedure could be applied, in which each independent macroscopically observed variable is assigned an uncertainty interval, and those micro-mechanical variables are chosen that minimize the sum of the squares of the weighted differences between the observed and the fitting values of the independent macroscopic variables, subject to the restriction (15) that $\theta_{sl} < 0$.

In applying the model, both the asymmetric and symmetric cases were considered. This is because even in configurations that are supposed to be symmetrical, low levels of asymmetry are practically present.

Before considering the data, exclude other possible flow fields. First, suppose the lower slip line lay *below* the fracture direction, but *above* the transverse direction, as shown in Fig. 4a. In contrast to the case of Fig. 2 analyzed above, slip on the lower line would turn out to

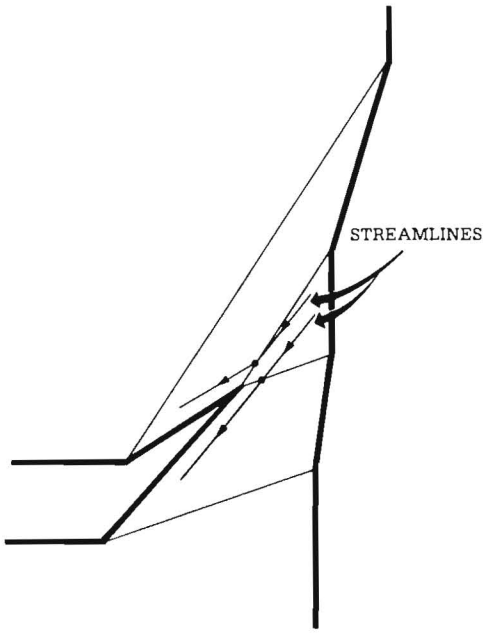

Fig. 4a. Streamlines for crack advancing between two slip lines with same sign of shear.

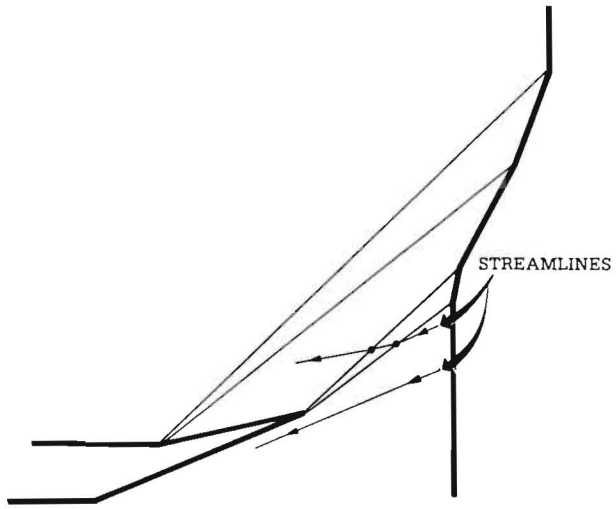

Fig. 4b. Streamlines for crack advancing below two slip lines with same sign of shear.

increase the lower projected ligament length above its original value. This was not observed, however.

Now assume that *both* slip lines lay *above* the fracture direction, as shown in Fig. 4b. In this field the deformation on the back surface is entirely above the point at which the crack breaks through to the back surface. In this case the new surface generated by sliding off lies entirely on the lower surfaces and the upper flank of the crack consists solely of fracture surface. Furthermore, the length and angle of the lower flank depend only on the resultant of slip on the two lines, not on their partitioning. In other words we could assume only a

single slip band. This simplified case cannot, obviously, account for the presence of a mode I component, as does the two slip-band model described above. It can be considered as a pure mode II limit (such a case was analysed in [5]).

As a final possibility, if the crack growth direction were to lie above both slip bands, crack closure would prevent any deformation.

3. Correlation with experimental results

Tensile tests on symmetrical and asymmetrical singly-grooved, fully plastic specimens were carried out on the six structural alloys summarized in Table 1. For a detailed description of the specimens and the test procedure, see [1]. The 1018 cold-finished and the HY-80 and HY-100 steels showed low strain hardening ($n \simeq 0.1$), the normalized 1018 and the hot rolled A36 steel showed higher hardening ($n \simeq 0.2$), and the 5086-H111 aluminum was intermediate. It was found that the lower hardening alloys exhibited a significantly lower ductility in the asymmetric configuration than the symmetric; the higher hardening alloys showed only a small reduction. After the test was completed, the profiles of the fracture surface and the deformed back surface were plotted with a travelling stage microscope to obtain the projected flank length ratios l_u/l_0, l_l/l_0, the flank angles θ_u, θ_l, and the upper back angle, β_u [1]. The projected length ratios depend on the strain hardening exponent, being smaller for a higher strain hardening. In the asymmetric case the lower projected flank is close to the original ligament length, especially with less hardening. These quantities are used in the model described above to yield the relative amounts of cracking and shearing, expressed as the ratios f/s_u, and s_l/s_u, the slip angles θ_{su} and θ_{sl} and the fracture angle θ_f.

Table 1. Room temperature tensile and hardness data for the six alloys tested

Yield		Tensile		Hardness	Fracture			Param. in $\bar{\sigma} = \bar{\sigma}_1(\varepsilon_0 + \bar{\varepsilon}^p)^n$		
Strength	Strain	Strength	Unif. strn		RA	true		Strength	Pre-strain	Exponent
						Strg	Strn			
Y.S.,	ε_y	T.S.,	ε_u	HDP		σ_f,	ε_f	σ_1	ε_0	n
MPa,	–	MPa,	–	Kgf/mm² %		MPa,	–	MPa	–	–
1018 steel (0.15–0.20% C, 0.60–0.90% Mn) cold finished										
411	0.002	500	0.04–0.086	180	52	660	0.72	590–690	−0.02–0.01	0.04–0.13
HY-80 steel (0.18% C, 2–3.25% Ni, 0.10–0.40% Mn, 0.15–0.35% Si)										
648	0.002	745	0.13	209	71	1200	1.25	1030–1150	0.007–0.043	0.10–0.17
HY-100 steel (0.20% C, 2.25–3.50% Ni, 0.10–0.40% Mn, 0.15–0.35% Si)										
772	0.002	869	0.072	248	71	1350	1.24	1100–1280	0.001–0.111	0.06–0.18
5086–H111 aluminium (4% Mg, 0.4% Mn, 0.15% Cr)										
225	0.002	333	0.15	82	44	480	0.58	510–540	0.002–0.010	0.15–0.18
1018 steel, normalized 1700° F in argon										
351 UYP										
305	0.028	457	0.17	103	70	830	1.19	690–770	−0.025–0.100	0.14–0.27
A36 steel (0.29% max C, 0.60–0.90% Mn) hot rolled										
411 UYP										
337	0.032	469	0.24	90	68	880	1.14	800–840	−0.020–0.022	0.20–0.26

Table 2. Characterization of singly-grooved *symmetrical* fracture

Alloy	1018 CF	HY-80	HY-100	5086-H111	1018 Norm.	A36 HR
Observations						
Projected flank ratio, $l_u/l_0 = l_l/l_0$						
	0.82	0.80	0.78	0.76	0.74	0.78
Upper flank angle, θ_u						
	−10°	−10°	−11°	−11°	−9°	−9°
Lower flank angle, θ_l						
	8°	16°	17°	9°	15°	11°
Upper back angle, β_u						
	12°	12°	13°	16°	15°	15°
Corresponding slip and fracture parameters (deduced)						
Lower slip angle, θ_{sl}						
	−37°	−46°	−44°	−23°	−20°	−29°
Upper slip angle, θ_{su}						
	35°	39°	39°	35°	40°	35°
Cracking angle, θ_f						
	−1°	7°	6°	−5°	−3°	−0.2°
Cracking parameter, f/s_u						
	2.91	2.36	2.00	1.79	1.41	2.09
Shearing parameter, s_l/s_u						
	1.02	1.13	1.09	0.90	0.81	0.94
Dependent variables						
Crack growth ductility, $D_g = u_y/l_0$						
deduced	0.26	0.37	0.39	0.27	0.32	0.28
load-ext	0.26	0.36	0.39	0.27	0.32	0.25
Apparent crack ductility on upper flank, $D_{AC,u}$						
deduced	0.24	0.28	0.32	0.33	0.36	0.30
SEM meas	0.67					0.68
Apparent crack ductility on lower flank, $D_{AC,l}$						
deduced	0.24	0.29	0.32	0.34	0.40	0.31
SEM meas	0.67					0.68
Upper shear band thickness, t_{su}/l_0						
	0.59	0.61	0.61	0.55	0.57	0.55
Upper shear band strain, γ_u						
	0.37	0.42	0.46	0.53	0.60	0.49
Lower shear band thickness, t_{sl}/l_0						
	0.58	0.74	0.71	0.41	0.44	0.51
Lower shear band strain, γ_l						
	0.39	0.39	0.43	0.64	0.63	0.49

The crack growth ductility D_g (or axial displacement u_y/l_0), the apparent crack ductility D_{AC}, and the shear band strain are also obtained from the model.

For *symmetrical specimens*, the results of the shear-band characterization are shown in Table 2. A slight asymmetry was always present, with the crack running a few degrees off the 0 deg (transverse) line, although the displacement vector was axial. The different levels of strain-hardening had little effect.

(a) There was some tendency for the *slip angles* θ_s to be within the non-hardening values of ± 45 deg, as observed previously (e.g. for annealed commercially pure aluminum [7]).
(b) The *crack growth ductilities* deduced from (4) all fell in the range of 0.24 to 0.39 and were within 0.03 of the observed values.

Table 3. Characterization of singly-grooved *asymmetrical* fracture

Alloy	1018 CF	HY-80	HY-100	5086-H111	1018 Norm.	A36 HR
Observations						
Projected upper flank ratio, l_u/l_0	0.92	0.89	0.89	0.89	0.83	0.84
Projected lower flank ratio, l_l/l_0	0.99	0.98	0.98	0.98	0.96	0.97
Upper flank angle, θ_u	40°	39°	39°	39°	36°	36°
Lower flank angle, θ_l	41°	41°	41°	41°	42°	41°
Back angle, β_u	15°	15°	14°	16°	13°	13°
Corresponding slip and fracture parameters (deduced)						
Lower slip angle, θ_{sl}	−17°	−19°	−10°	−26°	−40°	−39°
Upper slip angle, θ_{su}	47°	49°	49°	48°	53°	52°
Cracking angle, θ_f	40°	40°	40°	40°	39°	38°
Cracking parameter, f/s_u	10.20	6.83	6.71	6.93	3.57	3.92
Shearing parameter, s_l/s_u	0.09	0.13	0.12	0.14	0.18	0.15
Dependent variables						
Crack growth ductility, $D_g = u_y/l_0$						
deduced	0.09	0.13	0.13	0.13	0.26	0.23
load-ext	0.07	0.10	0.10	0.11	0.22	0.18
Apparent crack ductility on upper flank, $D_{AC,u}$						
deduced	0.005	0.010	0.012	0.008	0.012	0.010
SEM meas	0.37					0.57
Apparent crack ductility on lower flank, $D_{AC,l}$						
deduced	0.09	0.13	0.12	0.13	0.22	0.20
SEM meas	0.52					0.68
Upper shear band thickness, t_{su}/l_0	0.15	0.19	0.20	0.18	0.30	0.29
Upper shear band strain, γ_u	0.81	0.88	0.82	0.93	0.93	0.89
Lower shear band thickness, t_{sl}/l_0	1.11	1.12	1.00	1.19	1.28	1.27
Lower shear band strain, γ_l	0.009	0.019	0.020	0.019	0.041	0.031

(c) The deduced *apparent crack ductilities* D_{AC} on either the upper or lower flank were all between 0.24 and 0.40, a factor of about two below the observed values [6]. This indicates that the local process was by no means as well characterized as the macroscopic one.

For *asymmetrical specimens*, the results of the shear-band characterization are shown in Table 3. Here the different levels of strain-hardening had a substantial effect.

(a) In the higher hardening alloys the *cracking ratio* f/s_u is smaller by about a factor of two than in the lower hardening alloys. Also, the *shearing ratio* s_l/s_u is larger in the higher

hardening case. This indicates a larger contribution of the lower shear band to the deformation process in the high hardening case. Furthermore, the upper slip angle θ_{su} is larger than 45 deg. Both the upper and the lower slip angles increase in absolute value with higher hardening. All these indicate a higher mode I component in the high hardening case.

(b) The *shearing ratio* s_l/s_u is found to be 0.1–0.2, indicating that shearing in the upper slip band s_u (producing the lower flank) is about 5–10 times that in the lower slip band s_l (producing the upper flank).

(c) The deduced *crack growth ductility* D_g is 0.09 to 0.26, 20–30 percent above the values observed from the load-extension curves. Both the deduced and the observed values decrease by a factor of 2–3 for lower strain-hardening.

(d) The deduced *apparent crack ductility* on both the upper and the lower flank, as with symmetrical specimens, is much less than observed, especially on the upper flanks, which according to the model are formed almost entirely by fracture. Thus the micromechanics of the fracture process zone itself still must be worked out to link the far-field model to the fractographic observations. The correct trends are present, however, with more apparent crack ductility on the lower surface than the upper, and more with higher hardening than with lower hardening.

4. Conclusions

Fully plastic crack growth in singly-grooved tensile specimens was modelled by a combination of fracture on one plane and slip on another pair, for both the symmetric and asymmetric configurations. Macroscopic measurements allow characterizing the crack growth locally by the directions and amounts of fracture and slip. The model also gives other macroscopic quantities, such as the angle of the deformed surface on the back side of the specimen and the crack growth ductility, defined as the axial displacement per unit ligament reduction (as observed by the fractional drop in the load during crack growth). The crack growth ductility is of practical importance in determining the stiffness of the surrounding structure that is needed to prevent unstable fracture. This two slip plane model accounts for the presence of a mode I component that was experimentally confirmed in the asymmetric case.

Applied to six different structural alloys with strain-hardening exponents from 0.1 to 0.2, the model gave crack growth ductilities within 10 percent for the symmetrical configurations, where the values ranged from 0.25 to 0.40 and were unrelated to the strain-hardening exponent. For the asymmetrical configurations (that could occur near welds or shoulders), the crack growth ductility for the low hardening materials drops to 0.07 to 0.11 for the low-hardening alloys. The predicted values were within 30 percent of the observed ones. The slip-band model thus provided a good relative ranking of materials in regard to this important loss of ductility.

This slip plane model of fully plastic crack growth therefore provides a useful correlation between macroscopic measurements made on the specimens after fracture, and the loss of crack growth ductility that occurs in asymmetric configurations with materials with low strain hardening.

Acknowledgements

The financial support of the Office of Naval Research, Arlington, Virgina, Contract N00014-82K-0025, and the interest of the Project Monitor, Dr Y. Rajapakse, are gratefully acknowledged.

References

1. G.A. Kardomateas and F.A. McClintock, *International Journal of Fracture* 35 (1987) 103–124.
2. G.A. Kardomateas, Chapter 6 in "Mixed Mode I and II Fully Plastic Crack Growth from Simulated Weld Defects", Ph.D thesis, Department of Mechanical Engineering, Massachusetts Institute of Technology, Cambridge, Massachusetts (1985).
3. P. Ponte-Castañeda, *Journal of the Mechanics and Physics of Solids* 35 (1987) 227–268.
4. F.A. McClintock, in *Fracture*, Vol. 3, H. Liebowitz (ed.), Academic Press, New York (1970) 47–225.
5. G.A. Kardomateas, *Journal of Engineering Materials and Technology* (*ASME*) 108 (1986) 285–289.
6. G.A. Kardomateas, *Scripta Metallurgica* 20 (1986) 609–614.
7. F.A. McClintock and A.S. Argon, *Mechanical Behaviour of Materials*, Addison-Wesley, Reading, Massachusetts (1966) 324.

Résumé. Dans ce travail, on caractérise la croissance complètement plastique d'une fissure dans des éprouvettes de traction à rainure simple en état plan de déformations par les directions et l'intensité de la rupture et des glissements selon les trois plans de référence. Ce modèle fournit la ductilité vis-à-vis de la croissance d'une fissure, définie comme le déplacement axial par unité de réduction de ligament, en fonction des longeurs et directions de la surface de rupture, ainsi que la déformation de la surface arrière. Cette ductilité présente une importance pratique pour la détermination de la raideur de la structure d'environnement nécessaire pour éviter une rupture instable. Le modèle fournit également les directions et amplitudes des glissements et de la rupture.

Appliqué à six alliages de construction aux modules d'écrouissage compris entre 0.1 et 0.2, le modèle fournit les ductilités vis-à-vis de la croissance d'une fissure avec un écart de 10% par rapport à celles observées dans des configurations symétriques où les valeurs, non liées aux modules d'écrouissage, s'étalent entre 0.25 et 0.40. Pour des configurations asymétriques, telles qu'on les rencontre près des soudures ou dans les épaulements, la ductilité vis-à-vis de la croissance des fissures tombe à des valeurs de 0.07 à 0.11, dans le cas de matérizux à faible écrouissage. Les valeurs prédites, plus élevées dans les alliages fortement sensibles au vieillissement, s'écartent de 30% des valeurs observées. Ainsi, le modèle à plans de glissement d'une croissance complètement plastique d'une fissure fournit une corrélation utile entre des mesures macroscopiques sur éprouvettes après rupture et l'importante perte de ductilité vis-à-vis de la croissance d'une fissure, rencontrée dans des configurations asymétriques totalement plastiques avec des matériaux à faible sensibilité à l'écrouissage.